Brain Cortical Functional Gradients Predict Cortical Folding Patterns via Attention Mesh Convolution

Li Yang[1], Zhibin He[1], Tianyang Zhong[1], Changhe Li[1], Dajiang Zhu[2], Junwei Han[1], Tianming Liu[3], and Tuo Zhang[1]

[1] Northwestern Polytechnic University, Xi'an, China
[2] University of Texas at Arlington, TX, USA
[3] University of Georgia, GA, USA
tuozhang@nwpu.edu.cn

Abstract. Research has shown a strong link between brain function and cortical folding using various imaging techniques and genetics. Understanding the functional roles of gyri and sulci in cortical folding patterns is crucial for insights into biological and artificial neural networks. However, the complex relationship, individual variations, and intricate brain function distribution pose challenges in developing a comprehensive theory and computational model. To address this, a new model leveraging brain functional gradients from fMRI data was developed to predict individual cortical folding maps. The model incorporates attention mesh convolution to account for spatial organization, showing superior performance compared to existing models. Discoveries indicate that less dominant functional gradients play a significant role in folding prediction, with cortical landmarks found on borders of activated regions. The results highlight the potential of tailored neural networks in enhancing the understanding of brain anatomy-function relationships.

Keywords: Brain function · Cortical folding · Mesh convolution.

1 Introduction

Relation between brain function and cortical folding has long been intriguing due to its importance in offering profound insight into brain functional operation mechanisms, brain development and evolution, as well as being of clinical applications [1]. Gyri and sulci, the convex and concave cortical folding patterns, are two basic anatomical units of cortical morphology. It has been found that gyri/sulci align well with cortical functional boundaries [2], at least in primary functional cortex. Specific gyro-sulcal patterns, such as the *plis de passage* gyri [3], topology of local gyri and sulci (such as H-shape sulci in frontal lobe [1], H-shape gyri in fusiform gyri [4] and the ventromedial prefrontal cortex (vmPFC) in DMN region [5]), were suggested to correspond to subtypes of a specific function (such as cognitive and perception ability associated with frontal lobe and reading ability associated with fusiform gyri) or relate to the placement of a specific functional region

(such as functional activation location in vmPFC). In [6], functional MRI signals were suggested to have stronger low frequency components on gyri, whereas sulci have signals of stronger high frequency components. Neuronal difference in their distributions [7], types [8], wiring patterns [9] and even morphology [7] were reported to be present between gyri and sulci, which was further suggested to lead to differentiated cell-level functioning patterns. In addition, expression of a huge number of genes was reported to be different between gyri and sulci [10]. Among them, interestingly, the same group of genes can lead to the formation of gyri/sulci on gyrencephalic species while mediating brain function distribution patterns on lissencephaly species [10], suggesting a possible deeply rooted bond between cortical folding pattern and brain functions. Importantly, the functional differentiation between gyri and sulci could also provide clues to artificial neural network design. For example, gyri were suggested to serve as functional hubs and sulci as local processors, whereas sulci were isolated by gyri on the cortical sheet [11]. Recalling that graph architecture of an artificial neural network in the sweet spot resembles the real neural networks [12], such a gyro-sulcal (hub-nonhub) spatial distribution might suggest an alternative approach for neural network design.

In spite of the importance in anatomy-function relation, no explicit explanation or generic theory of such a relation can be satisfactorily applied across brain regions and species [2][13]. Also, very few computational models are found [6] to provide a precise prediction from brain function to cortical folding. The reasons could be attributed to many folds: 1) the mapping between brain function and folding pattern is far from linear; 2) inter-individual variabilities are huge in the layout of both gyro-sulcal patterns and functional regions [2][13]; 3) brain function was usually delineated by atlases where "abrupt" boundaries were used to segregate functional "units" or "networks", the functional attributes within which were considered to be of the same. However, the transition of a brain function from one to another was suggested to be "smooth" and "gradual", which also gains supports from the related genetic expression [14]; 4) the spatial patterning of brain function distribution was not fully used to predict cortical folding.

To answer the aforementioned questions, as a preliminary effort, we proposed to use artificial neuronal networks to investigate the predictive ability of brain functional gradients on cortical folding patterns at the macro scale. By means of resting-state fMRI (rsfMRI) and structural MRI (sMRI) in the Human Connectome Project (HCP) dataset [15], we estimated the global functional gradients, embedding axes that encode the "gradual" differences in mesh vertices' connectivity patterns and can be present on a cortical sheet (top-left in Figure 1a), where the prediction of gyro-sulcal segmentation (top-right in Figure 1a) was performed. Technically, we proposed to use a mesh convolution model [16] based on the classic U-net architecture, which has been widely and successfully applied to medical image segmentation. In addition, to enhance the interpretability of the mapping from functional gradients to cortical folding maps, we added a channel attention block [17] to the head of the U-net mesh convolution model, where functional gradients, as multi-channels, were re-weighted by the attention block

before being fed to mesh convolution. The weights can encode the contribution of functional gradients to cortical folding prediction.

2 Related Works

2.1 Mesh Convolution

Meshes are composed of three distinct types of geometric primitives: vertices, edges, and faces. The classification on meshes is a basic research area which has made great progress with the development of deep learning. DiffusionNet [18] introduces a general-purpose approach to deep learning on 3D surfaces. The networks can be discretized on various geometric representations such as triangle meshes or point clouds, and can even be trained on one representation and then applied to another. HodgeNet [19] uses many features that make it an attractive alternative for learning from meshes. During inference, its structure resembles that of most spectral geometry processing algorithms: construct a useful operator, and compute features from its spectrum. However, the above two approaches, as well as many other methods, including Pointnet [20], MeshCNN [21], PD-MeshNet [22], MeshWalker [23], PFCNN [24], need geometric features of meshes, such as coordinates of vertices, which is not applicable to our task that learns and predicts "texture" features on meshes. BrainSurfCNN [25] and SubdivNet [16] provides a solution to the problem. BrainSurfCNN is a method which uses spherical convolutional kernel [26] to predict the task fMRI contrasts from resting-state functional connectivity ones under a regression framework. The work in [26] uses only one-ring neighborhood for convolution, which limits the extraction of long-range features. SubdivNet [16] uses a regular and uniform downsampling scheme to establish a fine-to-coarse mesh hierarchy. The convolutions efficiently support stride and large dilation, allowing the model to better capture long-range features.

2.2 Predicting Gyro-sulcus From fMRI

So far, there are very few works in predicting cortical folding pattern from fMRI via a deep learning model. Liu and colleagues [6] designed a convolutional neural network (CNN) based classifier, which can differentiate gyral and sulcal fMRI signals with a reasonable accuracy (0.67 on resting state fMRI). However, in this model, vertices on surfaces are samples (with a gyrus/sulcus label) independent from each other, whereas functional regions are not spatially isolated and independent. Either functional network studies or functional gradient ones demonstrated that remote or neighboring regions cooperate with each other to elicit and maintain a brain function [14][27]. Therefore, functional connectivity induced gradients that encode the spatial embedding of brain neuronal interactivity could be more suitable for prediction of spatial layout of gyri/sulci. Also, the relatively lower classification accuracy in [6] could be ascribed to the direct use of noisy fMRI signals as predictive features, whereas connectivities could mitigate such side effects and direct the attention to brain functions at a global scale rather than a vertex-wise one.

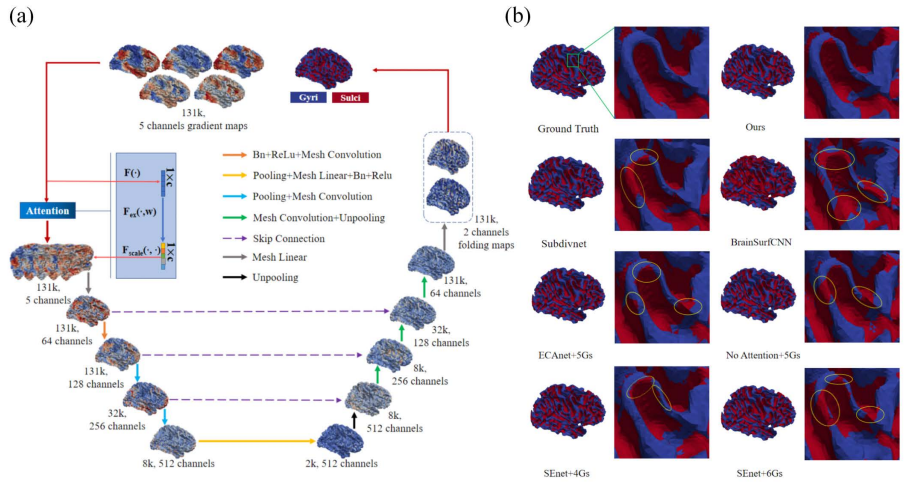

Fig. 1. a.Attention mesh convolution network architecture. b.Comparison experiments between ground truth and predicated results *via* different methods. A 'U' shaped gyral area is enlarged for inspection in detail, where yellow circles highlight the unsatisfied predictions. Abbreviations: G for gradients.

3 Method

In general, we designed a novel attention mesh convolution method based on U-net architecture to predict the gyro-sulcal segmentation map from brain functional gradient maps. The model's inputs are multi-channel functional gradients on icosahedral mesh [28], while its output is a two-channel binary map on the same icosahedral mesh (Figure 1a). More details about functional gradients and cortical folding patterns please referred to the supplementary.

3.1 Channel Attention Block

In order to boost the representation power of a network, the channel attention block SEnet [17] was applied in front of mesh convolution. In this attention block, a self-gating mechanism based on channel dependence yields the excitation of each channel (functional gradient in this work), such that channels of input were then re-weighted and fed to the following layers. This weight vector w could encodes the respective contribution of functional gradients to folding pattern prediction.

As shown in Figure 1a and Equation(1&2), the $\mathbf{F}(\cdot)$ is global average pooling function which compresses the characteristics of each channel into a real number, where c denotes the channel number, N_f denotes the number of mesh faces, G_c denotes the channel's gradient contrasts. Then, a $1 * \mathrm{c}$ vector was sent to $\mathbf{F}_{\mathrm{ex}}(\cdot, \mathrm{w})$ which was implemented by a fully connected layer. In our method, we

encoded 5 channels to 2 channels and then decoded them back to 5, in which w is a learnable parameter. After these operations, w gained the weight for every input channel, and then $\mathbf{F}_{\text{scale}}(\cdot,\cdot)$ scaled the $1 * \mathrm{c}$ vector and make the gradient contrasts on every mesh face multiplied by the corresponding channel weight. Finally, the re-weighted channels were fed to the mesh U-Net.

$$z = \mathbf{F}(\mathbf{G}_c) = \frac{1}{N_f}\sum_{i=1}^{N_f} G_c(i) \tag{1}$$

$$\mathbf{s} = \mathbf{F}_{ex}(\mathbf{z}, \mathbf{W}) = \sigma(g(\mathbf{z}, \mathbf{W})) = \sigma\left(\mathbf{W}_2 \delta\left(\mathbf{W}_1 \mathbf{z}\right)\right) \tag{2}$$

3.2 Mesh CNN with U-net Architecture and Loss Function

As shown in Figure 1a, after the attention block, a 'meshlinear' operation was used to generate 64 channels. This operation is a linear operation on meshes which resembles '1D' convolution on images. Then, the results above were sent to the classic U-Net framework. The kernel size was set to 3 on all mesh convolution operations, which was designed in [16], and the 'mean pooling' was used for downsampling. A difference between the classic U-Net framework and ours is that a 'meshlinear' operation was used after the third 'pooling' operation (yellow arrow in Figure 1a), and we found this change improves the accuracy of prediction. Finally, the deep network yielded two output channels. The loss was calculated by cross-entropy cost function, and the final result was obtained by an 'argmax' function, in which each mesh face was classified as sulcus or gyrus (Equation(3)).

$$L = -[y \log \widehat{y} + (1-y)\log(1-\widehat{y})] \tag{3}$$

The segmentation accuracy was defined in Equation(4), in which the N_f denotes the number of mesh faces, $\mathbf{prd_i}$ and $\mathbf{lab_i}$ denotes the *ith* face's prediction and label, respectively. *sign* function outputs 0 and 1, according to whether $\mathbf{prd_i}$ is equal to $\mathbf{lab_i}$ or not.

$$Acc = \frac{1}{N_f}\sum_{i=1}^{N_f} sign(\mathbf{prd}_i, \mathbf{lab}_i) \tag{4}$$

4 Experiments

4.1 Dataset, Preprocessing & Implementation

We used the 3-Tesla T1-weighted MRI and resting-state fMRI (rsfMRI) data from Human Connectome Project (HCP) dataset [15]. These data have been minimally pre-processed upon release [29]. More details of dataset and preprocessing can be found in supplementary. To adapt to the requirement in Subdivnet, we re-meshed the original surface and transferred the gradient features as well as class labels (0 for gyri and 1 for sulci) from mesh vertices to the mesh faces. Our experiments included 348 samples for training/testing (0.8/0.2), the batch size and learning rate was set to 6 and 0.01, respectively.

4.2 Results & Methods Comparison

Since our model was modified from Subdivnet [16], it was used as a mesh convolution baseline. The BrainSurfCNN [26] predicts the task fMRI contrasts from resting-state functional connectivity ones by using a regression scheme. For a fair comparison, we modified its' network architecture by replacing the 100 input channels with 5 channels, the 47 output channels with 2 channels in our model, as well as the loss function with cross-entropy loss, to implement the same segmentation task. The features on the mesh vertices were transferred to faces as well. Support-vector machine (SVM) was also selected for comparison. Figure 1b shows the segmentation results from one random testing subject and Table 1 reports the comparison of results *via* different methods by means of a variety of metrics. It is found that nonlinear models overwhelmingly outperform linear SVM in all metrics. Besides the intrinsic nonlinear relation between function and folding that could be significantly better encoded and decoded by nonlinear models, the definition of neighboring mask, a key factor for convolution operations on a mesh, could play an important role in the improvement. The importance of the convolution mask was also supported by a better performance of Subdivnet than BrainSurfCNN, since BrainSurfCNN, unlike Subdivnet, only used a small neighborhood as convolution mask which limits the extraction of long-range features. It is also found that sulci were often oversegmented by Subdivnet and BrainSurfCNN (yellow circles in Figure 1b) in highly bent gyral regions, where the cortical morphology is far more complex than others.

Table 1. Comparison with other methods. The MIoU, Precision, F1-score, Recall and Accuracy are reported.

Method	MIoU	Precision	F1-score	Recall	Accuracy
Our Method	0.603	0.752	0.751	0.750	75.85%
Subdivnet	0.595	0.744	0.745	0.746	75.11%
BrainSurfCNN	0.464	0.657	0.622	0.626	65.03%
Linear SVM	0.295	0.488	0.371	0.499	59.09%

4.3 Ablation Study

We considered the effects of different types of attention models and the number of functional gradient channels. It is found in Figure 1b and Table 2 that adding channel attention block or switching to another one does not significantly improve the performance in MIoU, Precision, F1 and Recall, whereas the accuracy could be affected by the selection of a channel attention block. The choice or absence of a channel attention could yield wrong segmentation in "straight" gyral/sulcal regions (the left yellow circles in third row of Figure 1b). Neither fewer (4G) nor more (6G) functional gradients improve the segmentation performance. Misclassification with 4G and 6G was usually found on the border between gyri and

Table 2. Ablation study on attention block and gradients. The MIoU, Precision, F1-score, Recall and Accuracy are reported. Red and blue denote the best and the second-best results, respectively. Abbreviations: G for gradients.

Type	MIoU	Precision	F1-score	Recall	Accuracy
SEnet+5Gs	0.603	0.752	0.751	0.750	75.85%
ECAnet+5Gs	0.599	0.750	0.747	0.745	75.61%
No Attention+5Gs	0.598	0.748	0.747	0.746	75.45%
SEnet+4Gs	0.587	0.744	0.737	0.734	74.89%
SEnet+6Gs	0.580	0.732	0.732	0.732	73.86%
Dict	0.448	0.627	0.611	0.614	63.60%

sulci (yellow circles in the fourth row of Figure 1b). In addition, we replaced the input data with another dataset which was generated by sparse representation, group-wise spatial dictionary mentioned in [30]. FMRI of every subject was decomposed into 100 networks, then 100 features of every points on the mesh was fed to train. As shown in Table 2, the experimental results show that the above functional network representation can not predict cortical gyro-sulcal segmentation well('Dict' represents the group-wise spatial dictionary dataset).

5 Discussion

The attention block re-weights the five gradients. The latter gradients (3G and 5G) gain relatively higher weights (Figure 2(b)), and their similarity to curvature map (measured by Pearson correlation) is significantly lower than the dominant gradients (1G and 2G). These results suggest that the implicit relation between function and folding might not be encoded in dominant gradients. It is also interesting to find that some functional networks, which are not explicitly represented by input gradients, can be identified in activation maps in deep layers. As an example, the fronto-parietal network, one of the resting-state networks not present in the 5 gradients, were found in both encoding and decoding layers, as shown in Figure 2(a). Finally, the activation maps in the last two-channel layer, were related to folding landmarks, gyral peaks (local convexity maxima) and sulcal pits (local concavity maxima), which were obtained independent of curvature used to yield the output gyro-sulcal maps. These landmarks (blue bubbles in Figure 2(c), group-wise mean locations across subjects) are not located on the highly activated regions (red regions). On average, activation values on these landmarks are 0.46 ± 0.62 and 0.60 ± 0.55 ($p<0.05$, *via* unpaired t-test) on other regions (expect the gray background), suggesting that these landmarks might mark the borders of folding patterns that are highly correlated with brain functions.

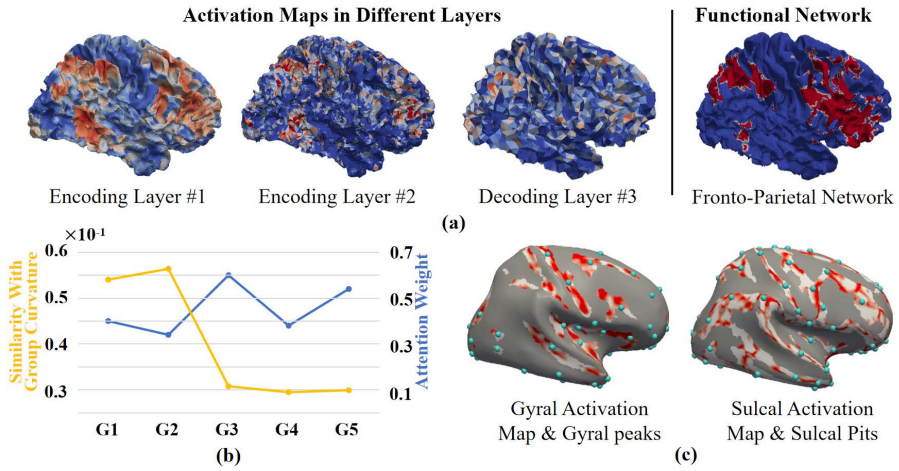

Fig. 2. (a) Activation maps in different deep layers that resemble the fronto-parietal functional network, not detected by functional gradients. (b) Similarity between functional gradients (G for short) and curvature map, and the weights of Gs learnt from attention block. (c) The segmentation activation maps (red for more activated regions) in the last two-channel layer and cortical landmarks (cyan bubbles), including gyral peaks and sulcal pits, that are independent from curvature.

6 Conclusion

In this work, we developed an attention mesh convolution model based on the U-net architecture to predict cortical gyro-sulcal segmentation maps from brain functional gradients derived from resting-state fMRI. The model architecture, such as input channel, output channel, feature types and attention block, can be easily extended or customized according to specific needs. Unlike the previous study, where functional signals from gyral/sulcal vertices were independently used as samples to a CNN model and their frequency band was found to be a discriminative feature [6], the mesh convolution in our model considers the spatial organization of functional gradients and folding patterns on a cortical sheet. The prediction performance *via* our model outperforms the state-of-the-art. In addition, we found that the dominant functional gradients contribute less to folding prediction. On the activation maps of the last layer, we found that some well-studied cortical landmarks are on the borders of, rather than within, the highly activated regions. These results and findings suggest that a specifically designed artificial neural network can improve the precision of the mapping between brain functions and cortical folding patterns, and can provide valuable clues of brain anatomy-function relation for neuroscience and artificial neural network design.

7 Acknowledgments

This work was supported by the National Natural Science Foundation of China 62131009, the National Key R&D Program of China under Grant 2020AAA0105701, the National Science Foundation of China under Grant 61936007, U20B2065, and U1801265.

8 Disclosure of Interests

The authors declare they have no competing interests.

References

1. Vanessa Troiani, Marisa A Patti, and Kayleigh Adamson. The use of the orbitofrontal h-sulcus as a reference frame for value signals. *European Journal of Neuroscience*, 51(9):1928–1943, 2020.
2. Bruce Fischl, Niranjini Rajendran, Evelina Busa, Jean Augustinack, Oliver Hinds, BT Thomas Yeo, Hartmut Mohlberg, Katrin Amunts, and Karl Zilles. Cortical folding patterns and predicting cytoarchitecture. *Cerebral cortex*, 18(8):1973–1980, 2008.
3. Jean Régis, Jean-François Mangin, Taku Ochiai, Vincent Frouin, Denis Rivière, Arnaud Cachia, Manabu Tamura, and Yves Samson. "sulcal root" generic model: a hypothesis to overcome the variability of the human cortex folding patterns. *Neurologia medico-chirurgica*, 45(1):1–17, 2005.
4. Arnaud Cachia, Margot Roell, Jean-François Mangin, Zhong Yi Sun, Antoinette Jobert, Lucia Braga, Olivier Houde, Stanislas Dehaene, and Grégoire Borst. How interindividual differences in brain anatomy shape reading accuracy. *Brain Structure and Function*, 223(2):701–712, 2018.
5. Alizée Lopez-Persem, Lennart Verhagen, Céline Amiez, Michael Petrides, and Jérome Sallet. The human ventromedial prefrontal cortex: sulcal morphology and its influence on functional organization. *Journal of Neuroscience*, 39(19):3627–3639, 2019.
6. Huan Liu, Shu Zhang, Xi Jiang, Tuo Zhang, Heng Huang, Fangfei Ge, Lin Zhao, Xiao Li, Xintao Hu, Junwei Han, et al. The cerebral cortex is bisectionally segregated into two fundamentally different functional units of gyri and sulci. *Cerebral Cortex*, 29(10):4238–4252, 2019.
7. Claus C Hilgetag and Helen Barbas. Developmental mechanics of the primate cerebral cortex. *Anatomy and embryology*, 210(5):411–417, 2005.
8. Brian G Rash, Alvaro Duque, Yury M Morozov, Jon I Arellano, Nicola Micali, and Pasko Rakic. Gliogenesis in the outer subventricular zone promotes enlargement and gyrification of the primate cerebrum. *Proceedings of the National Academy of Sciences*, 116(14):7089–7094, 2019.
9. Gang Xu, Andrew K Knutsen, Krikor Dikranian, Christopher D Kroenke, Philip V Bayly, and Larry A Taber. Axons pull on the brain, but tension does not drive cortical folding. *Journal of biomechanical engineering*, 132(7), 2010.
10. Camino de Juan Romero, Carl Bruder, Ugo Tomasello, José Miguel Sanz-Anquela, and Víctor Borrell. Discrete domains of gene expression in germinal layers distinguish the development of gyrencephaly. *The EMBO journal*, 34(14):1859–1874, 2015.

11. Fan Deng, Xi Jiang, Dajiang Zhu, Tuo Zhang, Kaiming Li, Lei Guo, and Tianming Liu. A functional model of cortical gyri and sulci. *Brain structure and function*, 219(4):1473–1491, 2014.
12. Jiaxuan You, Jure Leskovec, Kaiming He, and Saining Xie. Graph structure of neural networks. In *International Conference on Machine Learning*, pages 10881–10891. PMLR, 2020.
13. Martin A Frost and Rainer Goebel. Measuring structural–functional correspondence: spatial variability of specialised brain regions after macro-anatomical alignment. *Neuroimage*, 59(2):1369–1381, 2012.
14. Julia M Huntenburg, Pierre-Louis Bazin, and Daniel S Margulies. Large-scale gradients in human cortical organization. *Trends in cognitive sciences*, 22(1):21–31, 2018.
15. David C Van Essen, Stephen M Smith, Deanna M Barch, Timothy EJ Behrens, Essa Yacoub, Kamil Ugurbil, Wu-Minn HCP Consortium, et al. The wu-minn human connectome project: an overview. *Neuroimage*, 80:62–79, 2013.
16. Shi-Min Hu, Zheng-Ning Liu, Meng-Hao Guo, Jun-Xiong Cai, Jiahui Huang, Tai-Jiang Mu, and Ralph R Martin. Subdivision-based mesh convolution networks. *ACM Transactions on Graphics (TOG)*, 41(3):1–16, 2022.
17. Jie Hu, Li Shen, and Gang Sun. Squeeze-and-excitation networks. In *Proceedings of the IEEE conference on computer vision and pattern recognition*, pages 7132–7141, 2018.
18. Nicholas Sharp, Souhaib Attaiki, Keenan Crane, and Maks Ovsjanikov. Diffusionnet: Discretization agnostic learning on surfaces. *ACM Transactions on Graphics (TOG)*, 41(3):1–16, 2022.
19. Dmitriy Smirnov and Justin Solomon. Hodgenet: learning spectral geometry on triangle meshes. *ACM Transactions on Graphics (TOG)*, 40(4):1–11, 2021.
20. Charles R Qi, Hao Su, Kaichun Mo, and Leonidas J Guibas. Pointnet: Deep learning on point sets for 3d classification and segmentation. In *Proceedings of the IEEE conference on computer vision and pattern recognition*, pages 652–660, 2017.
21. Rana Hanocka, Amir Hertz, Noa Fish, Raja Giryes, Shachar Fleishman, and Daniel Cohen-Or. Meshcnn: a network with an edge. *ACM Transactions on Graphics (TOG)*, 38(4):1–12, 2019.
22. Francesco Milano, Antonio Loquercio, Antoni Rosinol, Davide Scaramuzza, and Luca Carlone. Primal-dual mesh convolutional neural networks. *Advances in Neural Information Processing Systems*, 33:952–963, 2020.
23. Alon Lahav and Ayellet Tal. Meshwalker: Deep mesh understanding by random walks. *ACM Transactions on Graphics (TOG)*, 39(6):1–13, 2020.
24. Yuqi Yang, Shilin Liu, Hao Pan, Yang Liu, and Xin Tong. Pfcnn: Convolutional neural networks on 3d surfaces using parallel frames. In *Proceedings of the IEEE/CVF Conference on Computer Vision and Pattern Recognition*, pages 13578–13587, 2020.
25. Gia H Ngo, Meenakshi Khosla, Keith Jamison, Amy Kuceyeski, and Mert R Sabuncu. From connectomic to task-evoked fingerprints: Individualized prediction of task contrasts from resting-state functional connectivity. In *International Conference on Medical Image Computing and Computer-Assisted Intervention*, pages 62–71. Springer, 2020.
26. Chiyu Jiang, Jingwei Huang, Karthik Kashinath, Philip Marcus, Matthias Niessner, et al. Spherical cnns on unstructured grids. *arXiv preprint arXiv:1901.02039*, 2019.
27. Jessica S Damoiseaux, SARB Rombouts, Frederik Barkhof, Philip Scheltens, Cornelis J Stam, Stephen M Smith, and Christian F Beckmann. Consistent resting-state networks across healthy subjects. *Proceedings of the national academy of sciences*, 103(37):13848–13853, 2006.

28. John R Baumgardner and Paul O Frederickson. Icosahedral discretization of the two-sphere. *SIAM Journal on Numerical Analysis*, 22(6):1107–1115, 1985.
29. Matthew F Glasser, Stamatios N Sotiropoulos, J Anthony Wilson, Timothy S Coalson, Bruce Fischl, Jesper L Andersson, Junqian Xu, Saad Jbabdi, Matthew Webster, Jonathan R Polimeni, et al. The minimal preprocessing pipelines for the human connectome project. *Neuroimage*, 80:105–124, 2013.
30. Lin Zhao, Huan Liu, Xi Jiang, Shijie Zhao, Zhibin He, Tianming Liu, Lei Guo, and Tuo Zhang. A task performance-guided model of functional networks identification. In *2019 IEEE 16th International Symposium on Biomedical Imaging (ISBI 2019)*, pages 1590–1593, 2019.